

## Abbreviations

AD	Axial diffusivity
ADC	Apparent diffusion coefficient
ADHD	Attention deficit hyperactivity disorder
BET	Brain extraction tool
CSF	Cerebrospinal fluid
DKI	Diffusion kurtosis imaging
DTI	Diffusion tensor imaging
DWI	Diffusion-weighted imaging
FA	Fractional anisotropy
MD	Trace, mean diffusivity
MRI	Magnetic resonance imaging
RD	Radial diffusivity
ROI	Region of interest
TBSS	Tract-based spatial statistics

---

## 5.1 Introduction

Diffusion tensor imaging (DTI) is an advanced magnetic resonance imaging (MRI) technique that provides detailed information about tissue microstructure such as fiber orientation, axonal density, and degree of myelination. DTI is based on the measurement of the diffusion of water molecules. It was developed in the early 1990s and since then has been applied in a wide

variety of scientific and clinical settings, especially, but not limited to, the investigation of brain pathology in schizophrenia (Shenton et al. 2001; Qiu et al. 2009, 2010), Alzheimer's disease (Damoiseaux et al. 2009; Mielke et al. 2009; Avants et al. 2010; Gold et al. 2010; Jahng et al. 2011), and autism (Pugliese et al. 2009; Cheng et al. 2010; Fletcher et al. 2010). This chapter describes the basics of the technique, outlines resources needed for acquisition, and focuses on post-processing techniques and statistical analyses with and without a priori hypotheses.

---

## 5.2 Basic Principles of Diffusion

### 5.2.1 Brownian Motion

Water molecules are constantly moving due to their thermal energy at temperatures above zero. In 1827, Robert Brown described the phenomena of particles suspended in fluid that move randomly (Brown 1827). Starting from the same position, the movement paths of single water molecules are unpredictable and end up in unforeseeable positions at time  $x$ . The process of diffusion depends upon a concentration gradient that was described by Fick's first law of diffusion. Fick's second law calculates the distance a particle diffuses in a certain time based on the diffusion coefficient (Fick 1855). Albert Einstein derived Fick's second law from thermodynamic laws, thereby building toward what has evolved

---

I.K. Koerte, MD (✉) • M. Muehlmann, MD  
Division of Radiology, Ludwig-Maximilians-  
University, Munich, Germany  
e-mail: [inga.koerte@med.lmu.de](mailto:inga.koerte@med.lmu.de);  
[muehlmann@bwh.harvard.edu](mailto:muehlmann@bwh.harvard.edu)

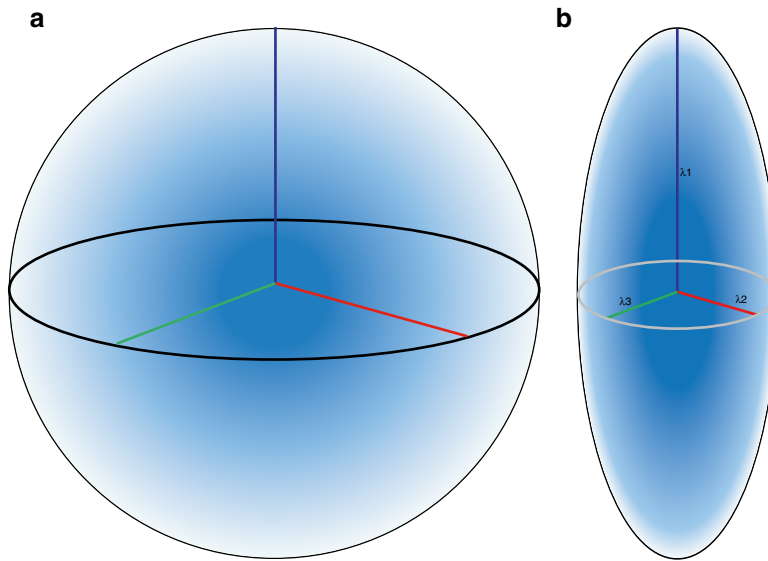


**Fig. 5.1** Isotropic and anisotropic diffusion

to diffusion theory. Further, Einstein was able to mathematically explain Brownian motion by determining the mean squared displacement of a single particle (Einstein 1905).

### 5.2.2 Isotropic Diffusion

During the process of diffusion, the random nature of Brownian motion causes molecules to move passively from a region with high concentration to a region with low concentration. If a drop of ink is dropped in a glass filled with water, the drop seems to stay steady in place at first, before it enlarges spherically until the entire water in the glass becomes homogeneously colored. While the mixing of the fluids ceases macroscopically as a result of the vanishing concentration gradient, the molecules keep randomly moving, which is also called self-diffusion. Looking at a large number of water molecules originating from the same position, we observe that the distribution of the end points after time  $x$  follows a 3D Gaussian distribution. This is also referred to as free, unrestricted, or isotropic diffusion (Fig. 5.1a).

Diffusion in biological tissues is affected by the microstructure of the respective tissue. In biological tissue, the water molecules still randomly diffuse in each 3D direction (isotropic) but are slowed down in their range due to collision with large-scaled biological molecules. Therefore, the diffusion coefficient for water in biological tissues, which is called apparent diffusion coefficient (ADC), is lower than in water. In an unorganized biological environment, ADC is independent from the direction of measurement, as a result of the spherical shape of diffusion. However, the radius of diffusion is reduced compared to unhindered diffusion when considering equal time points.

### 5.2.3 Anisotropic Diffusion

In highly structured biological tissues, such as white matter of the brain, the movement of water molecules is restricted by cell membranes, myelin sheaths, and microfilament (Jones et al. 2013). The diffusion probability of water molecules in structured tissue describes an ellipsoid based on the preferred diffusion direction parallel to the axon (Fig. 5.1b) (Basser et al. 1994a, b).

In organized tissues such as the white matter, the ADC depends on the direction from which it is measured. The ADC is higher if the diffusion gradients are aligned to the preferred diffusion direction and lower if measured perpendicular to it.

## 5.3 Magnetic Resonance Diffusion-Weighted Imaging

### 5.3.1 Magnetic Resonance Imaging

Magnetic resonance imaging (MRI) relies on the nuclear spin which is innate to all elements with an odd-numbered composition of nuclear particles in their nucleus (Rabi et al. 1938). One example is the hydrogen nucleus consisting of a single proton. The proton can be understood as a charged moving particle while the conical movement as described by its spin axis is called precession (Loeffler 1981). Tissues of the human body contain between 22 % (bones) and 95 % (blood plasma) water and are therefore rich in protons. In a static magnetic field, the spins are precessing parallel and antiparallel to the magnetic field axis. Both orientations can be understood as different states of energy, where the upward spins are on a lower energetic level compared to the downward spins. In order to keep the energetic balance, there are more upward-oriented spins. The surplus of spins oriented upward causes a constant magnetization along the axis of the static magnetic field ( $z$ -axis which is also called longitudinal magnetization). MRI uses radiofrequency pulses to disrupt the constant magnetization and tilt the spin axis into the  $xy$ -plane (transversal magnetization) (Loeffler 1981). The moving sum of magnetic vectors in the  $xy$ -plane induces an alternating voltage in the reception coil (MRI signal). The process in which the transversal magnetization returns to the longitudinal magnetization is accompanied with energy loss and is called spin-lattice relaxation or T1-relaxation. In contrast the T2-relaxation is caused by energetic shifts between the spins while dephasing, while no energy is getting lost to the surrounding (Loeffler 1981).

### 5.3.2 Diffusion-Weighted Imaging

In diffusion-weighted imaging (DWI), the strength of the MRI signal depends on the mean displacement of water molecules. Here a strong signal indicates a low diffusion in the direction of the magnetic gradient field. Accordingly, the signal loss is higher when the mean displacement of the water molecules is higher along the gradient. The mean displacement of water molecules is described as the apparent diffusion coefficient (ADC). In the clinical setting, DWI is often used in the assessment of stroke (Warach et al. 1995; Brunser et al. 2013) because extracellular diffusion restriction due to the swelling of neurons is a highly sensitive marker of cerebral ischemia. This was first described by Moseley in 1990 (1990).

#### 5.3.2.1 Stejskal-Tanner Sequence

To obtain diffusion-weighted images, the Stejskal-Tanner sequence is applied (Stejskal and Tanner 1965). A basic scheme of this sequence is given in Fig. 5.2. The process starts by applying a  $90^\circ$  radiofrequency pulse after time ( $t$ ) to shift the magnetization vector into the  $xy$ -plane. The equal precessing spins create a magnetic momentum that is rotating in the  $xy$ -plane thereby inducing a voltage that can be referred to as the MRI signal. Due to intermolecular interactions and also due to field inhomogeneity, the first equally precessing spins start to dephase, resulting in a decay of the T2 signal. Now a  $180^\circ$  radiofrequency pulse is applied to turn the whole spin magnetization around. Previously slower precessing spins are now put ahead of faster precessing spins. After time ( $2t = TE$ ), all spins precess in phase again, and the recovered magnetic momentum induces a voltage, the spin echo. One could also state that by using the  $180^\circ$  pulse, the effect of field inhomogeneities is reversed. For diffusion weighting, two magnetic gradients are applied in addition to the static magnetic field and the radiofrequency pulse (Stejskal and Tanner 1965). Here the first linear gradient weakens or strengthens the local field strength resulting in a certain position-dependent precession frequency of corresponding spins. For

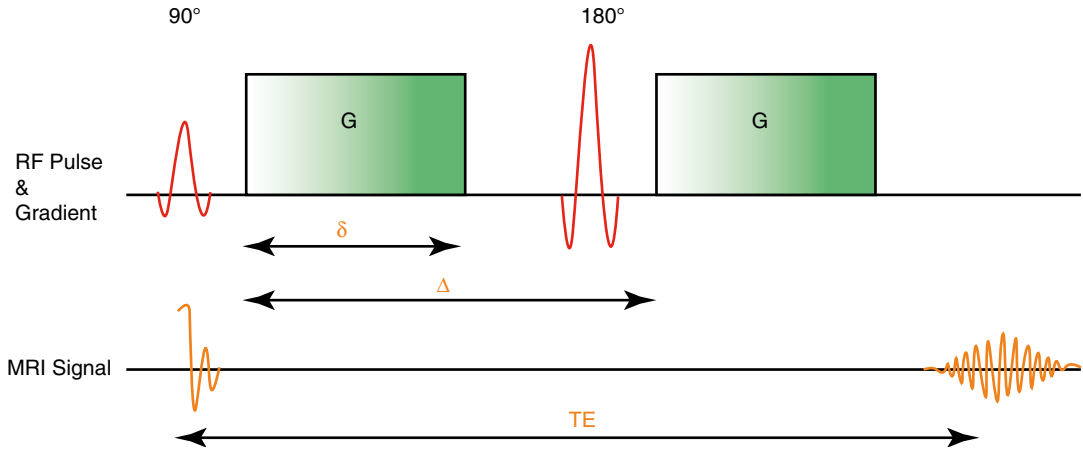


**Fig. 5.2** Stejskal-Tanner Sequence

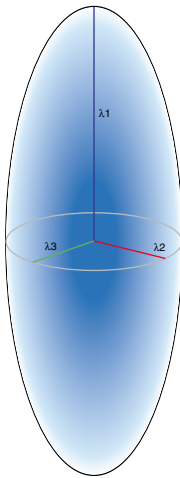


**Fig. 5.3** Eigenvalues of the diffusion ellipsoid

spins in solid tissue, the effect of this gradient whether weakened or strengthened is reversed by the second gradient pulse (Stejskal and Tanner 1965). The signal loss is larger in tissues where the containing spins can move more rapidly between the applications of both gradient pulses.

### 5.3.3 Diffusion Tensor Imaging

Diffusion tensor imaging (DTI) emerged from DWI in 1994 (Basser et al. 1994a, b). DTI is

also based on the diffusion of water molecules as acquired with the Stejskal-Tanner sequence. The main advantage over DWI is that it makes it possible to quantify not only the diffusion in total but also the directionality of diffusion, which is called the diffusion tensor. In order to quantify the diffusion tensor, six different diffusion measurements and directions are necessary to sufficiently satisfy the tensor equation (Pierpaoli et al. 1996). Information content and reliability of the calculation of the diffusion tensor can be further improved by increasing the number of diffusion directions. Moreover, for complex post-processing analyses such as tractography, at least 30 diffusion directions are recommended in order to obtain reliable results (Spiotta et al. 2012). Increasing the number of diffusion directions enhances the precision of the reconstruction while the statistical rotational variance is reduced (Jones et al. 2013). The 3D information obtained from various diffusion gradients is used to calculate a multilinear transformation, the diffusion tensor. The diffusion tensor can be described using eigenvalues and eigenvectors and visualized as the diffusion ellipsoid (Fig. 5.3). The axes of the three-dimensional coordinate system are called eigenvectors, while the length of their measure is called eigenvalues. The three eigenvalues are symbolized by the Greek letter lambda ( $\lambda_1$ ,  $\lambda_2$ ,  $\lambda_3$ ). The eigenvalues are then used to calculate different parameters of the diffusion tensor.

### 5.3.4 Quantitative Parameters of the Diffusion Tensor

Commonly used quantitative parameters of the diffusion tensor are axial diffusivity (AD); radial diffusivity (RD); trace, mean diffusivity (MD); and fractional anisotropy (FA). These parameters are calculated for each voxel of the imaging data set and make it possible to characterize, noninvasively, tissue on a microscopic level.

#### 5.3.4.1 Axial Diffusivity and Radial Diffusivity

The largest eigenvalue is named  $\lambda_1$  and is oriented parallel to the axonal structures. It is therefore equal to the diffusion tensor parameter axial diffusivity:

$$AD = \lambda_1$$

The eigenvalues  $\lambda_2$  and  $\lambda_3$  are the values along the two short axis of the coordinate system. They are therefore used to calculate the radial diffusivity which describes the diffusion perpendicular to the main diffusion direction. RD is calculated by dividing the sum of the short-axis eigenvalues by 2:

$$RD = \frac{(\lambda_2 + \lambda_3)}{2}$$

#### 5.3.4.2 Trace and Mean Diffusivity

The sum of all three eigenvalues is called trace. Mean diffusivity is obtained when trace is divided by three:

$$\text{Trace} = \lambda_1 + \lambda_2 + \lambda_3$$

$$MD = \frac{(\lambda_1 + \lambda_2 + \lambda_3)}{3}$$

#### 5.3.4.3 Fractional Anisotropy

The calculation of fractional anisotropy weighs the preferred component of diffusivity to obtain information about the quantity of directionality. Therefore, the square root of the diffusion differences

$$\left( \sqrt{(\lambda_1 - \lambda_2)^2 + (\lambda_1 - \lambda_3)^2 + (\lambda_2 - \lambda_3)^2} \right)$$

is used and then averaged by the square root of

sums of squares  $\left( \sqrt{(\lambda_1)^2 + (\lambda_2)^2 + (\lambda_3)^2} \right)$ . The

first term  $\left( \sqrt{\frac{1}{2}} \right)$  scales the FA to values between 0 and 1:

$$FA = \sqrt{\frac{1}{2}} \frac{\sqrt{(\lambda_1 - \lambda_2)^2 + (\lambda_1 - \lambda_3)^2 + (\lambda_2 - \lambda_3)^2}}{\sqrt{(\lambda_1)^2 + (\lambda_2)^2 + (\lambda_3)^2}}$$

Based on these DTI parameters, assumptions can be made regarding the microstructure of the brain such as the orientation and diameter of axons and their surrounding structures such as the myelin sheaths. For example, decreased RD and therefore higher FA can be based on increased axonal density, reduced axonal diameter, and thicker myelin sheaths (Song et al. 2002). A lower FA can be caused by a number of factors, for example, a larger axon diameter (Takahashi et al. 2002), a lower axon density (Takahashi et al. 2002), and/or increased membrane permeability. Increased mean diffusivity represents an increase in extracellular diffusion of water molecules and can be the result of, for example, vasogenic edema (Filippi et al. 2001).

## 5.4 Post-Processing of DTI Data

### 5.4.1 Quality of DTI Data

The first and one of the most important steps in post-processing diffusion MRI data is to check the quality of the acquired data. The importance of the quality check arises from the susceptibility of diffusion MR images to artifacts, for example, motion artifact and/or susceptibility artifacts. While there are no strict guidelines for the post-processing of DTI data or standardized quality assurance, it is recommended that manual inspection be performed on the data, slice by slice, in order to ensure that reliable results are obtained for all acquired diffusion directions. All regions of interest must also be free from any artifact to avoid possible confounds in the calculation of diffusion parameters.

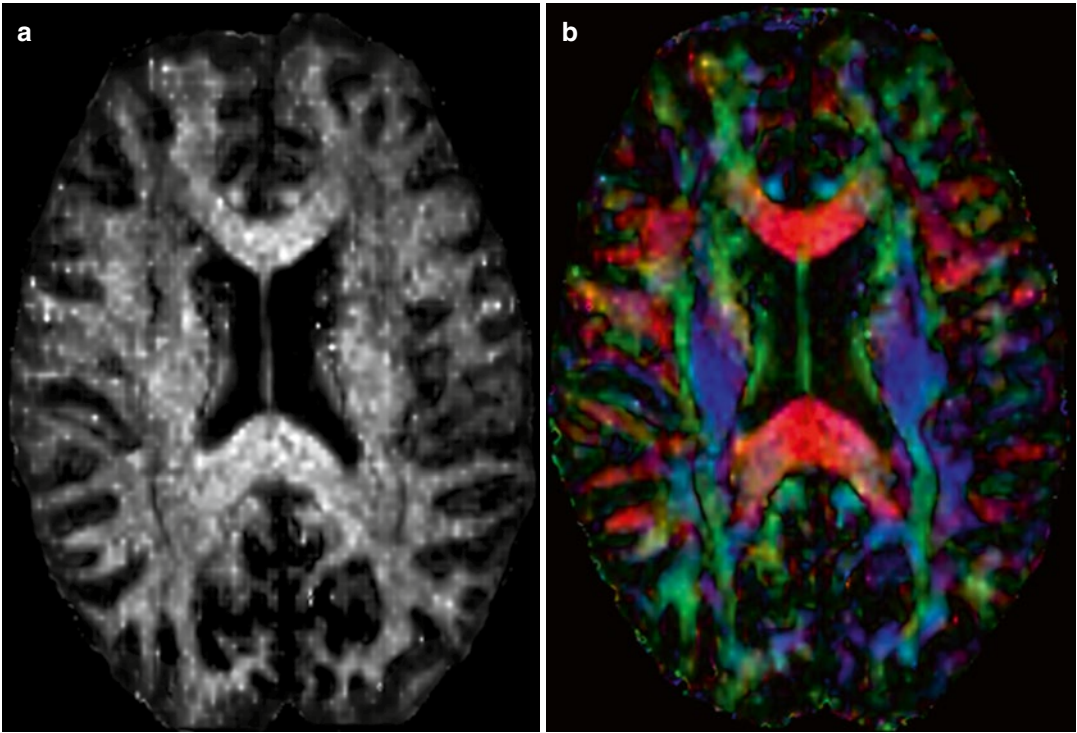


**Fig. 5.4** Scalar (a) and color-coded (b) FA maps

### 5.4.2 Diffusion Tensor Masks

Most post-processing techniques require a mask for the individual data set that contains only the brain and the surrounding cerebrospinal fluid (CSF) space. These masks can be obtained automatically using a software such as the brain extraction tool (BET), which is part of the FSL software (FMRIB Software Library, The Oxford Centre of Functional MRI of the Brain – FMRIB). To guarantee a high quality of data and to take the individual’s anatomy into account, the masks created automatically are then manually edited. The latter can be a labor-intensive process.

### 5.4.3 Visualization of DTI Parameters

The easiest way to visualize the DTI parameters is by displaying the value as the level of gray in each respective voxel (Fig. 5.4a). By adding the information of the main diffusion direction

using a color scheme, color-coded maps can be obtained (Fig. 5.4b). Blue-colored voxels represent the main diffusion direction parallel to the  $z$ -axis, that is, inferior to superior in human individuals. In contrast, the green-colored voxels represent the main diffusion direction parallel to the  $y$ -axis, that is, anterior to posterior. Red-colored voxels represent a main diffusion direction parallel to the  $x$ -axis, that is, left to right. While the axis and the directionality of diffusion in a specific tissue can be calculated, it is not possible to obtain information about the direction of the flow of actual information, which can occur bidirectionally.

### 5.4.4 Tract-Based Spatial Statistics

To investigate differences in DTI parameters between groups, a statistical approach can be used which takes all voxels of each individual into account. The most commonly used method is called tract-based spatial statistics (TBSS) (Smith et al. 2006), which is part of the freely avail-

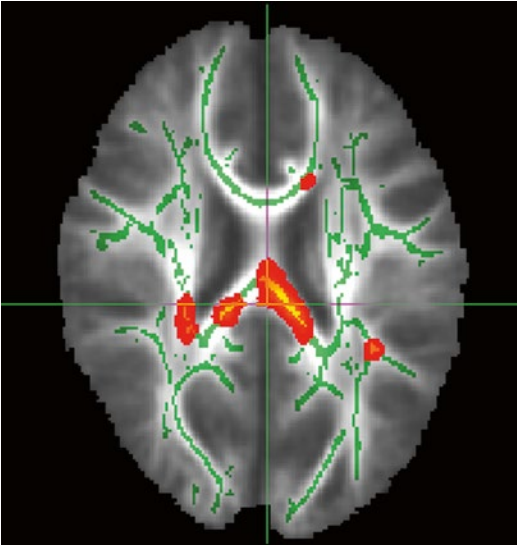


**Fig. 5.5** Example of significant TBSS result

able software package FSL (FMRIB Software Library, The Oxford Centre of Functional MRI of the Brain – FMRIB).

The individual DTI images are scaled to a standard space and aligned either to each other or to a standard image. After aligning the individual images, a three-dimensional map is created which then contains the mean of all individuals. This map can be used to calculate the mean skeleton representing the center elements of the main white matter tracts of all included individuals. TBSS uses a nonparametric statistical test that analyzes all voxels corresponding to the mean skeleton. Additional co-variables such as age or gender can be included in the analysis allowing for the investigation of dependencies. Results are corrected for multiple testing and are displayed in a 3D image (Fig. 5.5).

Advantages of using TBSS analysis include the possibility of testing without an a priori hypothesis and the possibility of including co-variables. Drawbacks of this voxel-wise approach are the loss of individual information due to partial volume effects and interindividual differences. One should also keep in mind that only the skeleton representing the main white matter tracts is analyzed, whereas voxels containing peripheral white matter or gray matter are not included. Additional caution should be taken

when investigating groups with a more heterogeneous anatomy such as children, especially when the age range is wide.

#### 5.4.5 Region-of-Interest Analysis

Region-of-interest (ROI) analyses are commonly used to test a priori hypotheses. They are performed at the level of the individual's data set. The ROI can be placed either manually or semiautomatically. When placing ROIs, special care should be taken to only include the structure of interest. Therefore, it is recommended that group standardized thresholds be used during the selection process to minimize partial volume effects. Partial volume effects result from the fact that a three-dimensional voxel can include variable amounts of information from both the structure of interest and the surrounding tissue. This can be done by using freely available software packages such as 3DSlicer (SPL, BWH, Harvard, Boston) (Fedorov et al. 2012) or FreeSurfer (NMR, MGH, Harvard, Boston) (Dale et al. 1999). ROIs can be analyzed with respect to their size and the mean of the respective diffusion parameter on the level of the individual. Obtained values can then be used for offline statistical analysis.

#### 5.4.6 Tractography

Tractography makes it possible to both visualize in three dimensions and quantify fiber tracts (Basser et al. 2000). Based on the preferred diffusion direction of neighboring voxels, the likelihood of (fiber) connectivity between the voxels can also be estimated. Fiber tracts can be identified by defining a single ROI as starting point or by using multiple ROIs that the fiber tract passes. The multiple ROI approach is especially useful to investigate long and complex tracts. Additional exclusion ROIs can be used to limit the obtained fibers, for example, when the corticospinal tract is of interest, fibers crossing to the other hemisphere may have to be excluded by an exclusion ROI in the sagittal midline. Tractography can be performed using the software 3DSlicer (Fedorov et al. 2012).

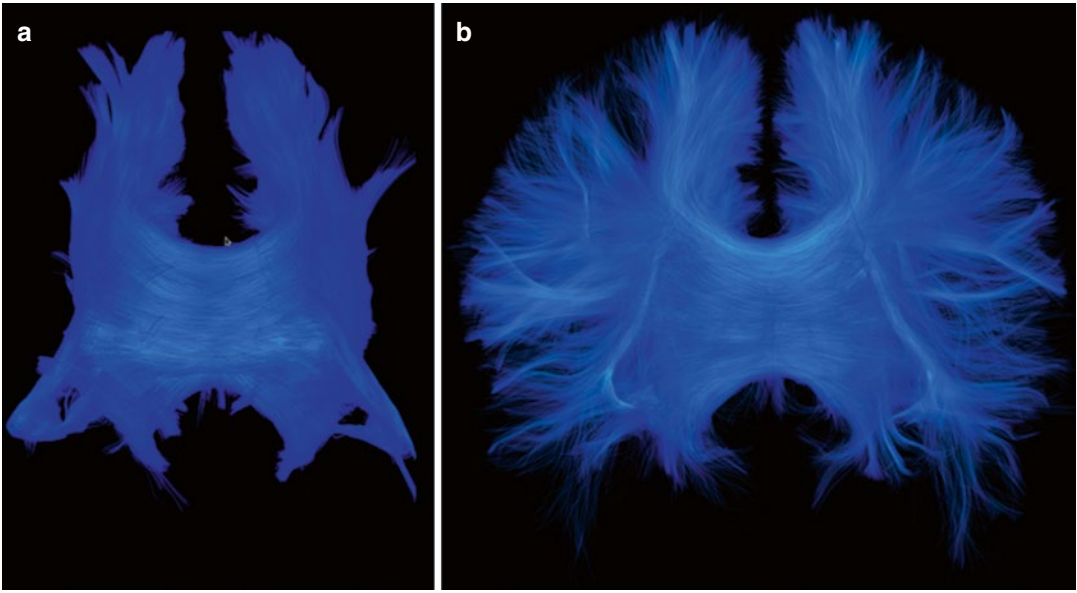


**Fig. 5.6** Single and Two-Tensor Tractography

Identified tracts can then be visualized. Moreover, the tract can be analyzed regarding the number of reconstructed fibers as well as their DTI parameters RD, AD, trace, MD, and FA. This makes tractography a more specific approach compared to ROI-based analyses or TBSS because only the structure of interest is analyzed. However, tractography is limited when it comes to crossing of fibers, for example, transcallosal fibers crossing the downward projecting cortico-spinal tract. This is because the tensor includes all information on the diffusion in the respective voxel assuming that all fibers in this voxel travel in the same direction. However, in large parts of the brain's white matter, voxels contain crossing fiber tracts that result in decreased anisotropy in a given voxel. This false decrease in anisotropy leads to fiber tracts ending abruptly. Multi-tensor algorithms calculate more than one tensor per voxel thereby making it possible to follow and to analyze tracts that travel in different directions (Fig. 5.6) (Malcolm et al. 2010).

## 5.5 Limitations

Limitations of DTI include the vulnerability to artifacts such as motion artifact, susceptibility artifact, and distortion artifact (eddy current).

To acquire DTI data covering the entire brain with high and reliable quality, a sequence takes between 5 and 10 min, which is relatively long compared to structural sequences such as T1-weighted and T2-weighted sequences. Especially in children and in the elderly, it can be difficult to obtain a complete DTI sequence without motion artifact.

Another limitation may be seen by the fact that the diffusion tensor is calculated for an entire voxel and therefore represents at least  $1 \text{ mm}^3$ , whereas the diameter of an axon is about  $7 \mu\text{m}$ . This means that DTI parameters may represent a combination of different structures rather than a single axon or fiber. However, to date, DTI is the most sensitive noninvasive technique that makes it possible to characterize microscopic brain white matter (Jones et al. 2013).

## 5.6 Future Directions

Although diffusion tensor imaging already looks back at close to two decades of success, there are still promising further developments regarding the acquisition of DTI data as well as post-processing techniques. Advanced post-processing algorithms using compressed sensing have been developed by Rathi et al. to enhance the quality



of images acquired with a lower number of diffusion directions in order to reduce the scanning time (Michailovich et al. 2011; Rathi et al. 2011). This advancement is of particular importance when investigating children, the elderly, and patients who have difficulties staying motionless in the scanner, for example, patients with Parkinson's disease, attention deficit hyperactivity disorder (ADHD), patients experiencing pain, or Alzheimer's disease.

Pasternak et al. have also introduced a new approach that makes it possible to differentiate two contributing compartments to the diffusion MRI signal (Pasternak et al. 2009). One compartment contains freely diffusing water molecules in the extracellular space, while the other compartment includes water molecules that are affected by structures in biological tissues. Therefore, this method enables the quantification of free water in the extracellular space and the assessment of tissue-specific, free-water-corrected FA and MD values (Pasternak et al. 2009). This method was recently applied to patients experiencing a first episode of schizophrenia where a widespread increase in free water was observed, suggesting a neuroinflammatory response, in addition to a reduction in free-water-corrected FA in the frontal regions of the brain, suggesting axonal degeneration (Pasternak et al. 2012).

Another promising approach is the diffusion kurtosis imaging (DKI). This approach is based on the multi-shell DWI, where multiple b-values are acquired in one session. In addition to common DTI parameters, the mean deviation from the Gaussian diffusion is calculated and taken into account. Cheung et al. were able to show higher sensitivity of kurtosis imaging compared with common DTI, in finding changes of white and gray matter during rat brain development (Cheung et al. 2009). Helpen used DKI to noninvasively compare the microstructural development of patients with ADHD compared to controls. Group comparison revealed that DKI-corrected RD and AD values stagnated in the ADHD group, while the control group showed an age-related increase in the complexity of white matter microstructure (Helpen et al. 2011). These preliminary results support the assumption that DKI may be a sensitive addition to DTI evaluation of white matter microstructure.

It is thus clear that there is much work to be done using diffusion measures in clinical populations and that this field is still in its infancy. A closer look at measures such as free water to delineate further possible neuroinflammatory versus neurodegenerative aspects of disease may provide important new insights as will the ability to more clearly specify the underlying changes by using DKI to specify further changes in the brain related to myelin disturbances. These advances, along with algorithms that greatly reduce the time in the magnet while providing the same information as acquisitions that by now take 60 min, will provide a level of sensitivity and specificity of pathology, in vivo, that is not possible today, although we are close.

---

## References

- Avants BB, Cook PA, Ungar L et al (2010) Dementia induces correlated reductions in white matter integrity and cortical thickness: a multivariate neuroimaging study with sparse canonical correlation analysis. *Neuroimage* 50(3):1004–1016
- Basser PJ, Mattiello J, LeBihan D (1994a) Estimation of the effective self-diffusion tensor from the NMR spin echo. *J Magn Reson B* 103(3):247–254
- Basser PJ, Mattiello J, LeBihan D (1994b) MR diffusion tensor spectroscopy and imaging. *Biophys J* 66(1):259–267
- Basser PJ, Pajevic S, Pierpaoli C et al (2000) In vivo fiber tractography using DT-MRI data. *Magn Reson Med* 44(4):625–632
- Brown R (1827) A brief account of microscopical observations made in the month of June, July and August 1827 on the particles contained in the pollen of plants and on the general existence of active molecules in organic and inorganic bodies. *Philos Mag* 4(4):161–173
- Brunser AM, Hoppe A, Illanes S et al (2013) Accuracy of diffusion-weighted imaging in the diagnosis of stroke in patients with suspected cerebral infarct. *Stroke* 44(4):1169–1171
- Cheng Y, Chou KH, Chen IY et al (2010) Atypical development of white matter microstructure in adolescents with autism spectrum disorders. *Neuroimage* 50(3):873–882
- Cheung MM, Hui ES, Chan KC et al (2009) Does diffusion kurtosis imaging lead to better neural tissue characterization? A rodent brain maturation study. *Neuroimage* 45(2):386–392
- Dale AM, Fischl B, Sereno MI (1999) Cortical surface-based analysis. I. Segmentation and surface reconstruction. *Neuroimage* 9(2):179–194
- Damoiseaux JS, Smith SM, Witter MP et al (2009) White matter tract integrity in aging and Alzheimer's disease. *Hum Brain Mapp* 30(4):1051–1059

- Einstein A (1905) Über die von der molekularkinetischen Theorie der Wärme geforderte Bewegung von in ruhenden Flüssigkeiten suspendierten Teilchen. *Ann Phys* 17:549–560
- Fedorov A, Beichel R, Kalpathy-Cramer J et al (2012) 3D Slicer as an image computing platform for the quantitative imaging network. *Magn Reson Imaging* 30(9):1323–1341
- Fick A (1855) Ueber diffusion. *Ann Phys* 170(1):59–86
- Filippi M, Cercignani M, Ingles M et al (2001) Diffusion tensor magnetic resonance imaging in multiple sclerosis. *Neurology* 56(3):304–311
- Fletcher PT, Whitaker RT, Tao R et al (2010) Microstructural connectivity of the arcuate fasciculus in adolescents with high-functioning autism. *Neuroimage* 51(3):1117–1125
- Gold BT, Powell DK, Andersen AH et al (2010) Alterations in multiple measures of white matter integrity in normal women at high risk for Alzheimer's disease. *Neuroimage* 52(4):1487–1494
- Helpert JA, Adisetiyo V, Falangola MF et al (2011) Preliminary evidence of altered gray and white matter microstructural development in the frontal lobe of adolescents with attention-deficit hyperactivity disorder: a diffusional kurtosis imaging study. *J Magn Reson Imaging* 33(1):17–23
- Jahng GH, Xu S, Weiner MW et al (2011) DTI studies in patients with Alzheimer's disease, mild cognitive impairment, or normal cognition with evaluation of the intrinsic background gradients. *Neuroradiology* 53(10):749–762
- Jones DK, Knosche TR, Turner R (2013) White matter integrity, fiber count, and other fallacies: the do's and don'ts of diffusion MRI. *Neuroimage* 73:239–254
- Loeffler W, Oppelt A (1981) Physical principles of NMR tomography. *Eur J Radiol* 1(4):338–344
- Malcolm JG, Shenton ME, Rathi Y (2010) Filtered multi-tensor tractography. *IEEE Trans Med Imaging* 29(9):1664–1675
- Michailovich O, Rathi Y, Dolui S (2011) Spatially regularized compressed sensing for high angular resolution diffusion imaging. *IEEE Trans Med Imaging* 30(5):1100–1115
- Mielke MM, Kozauer NA, Chan KC et al (2009) Regionally-specific diffusion tensor imaging in mild cognitive impairment and Alzheimer's disease. *Neuroimage* 46(1):47–55
- Moseley ME, Cohen Y, Mintorovitch J et al (1990) Early detection of regional cerebral ischemia in cats: comparison of diffusion- and T2-weighted MRI and spectroscopy. *Magn Reson Med* 14(2):330–346
- Pasternak O, Sochen N, Gur Y et al (2009) Free water elimination and mapping from diffusion MRI. *Magn Reson Med* 62(3):717–730
- Pasternak O, Westin CF, Bouix S et al (2012) Excessive extracellular volume reveals a neurodegenerative pattern in schizophrenia onset. *J Neurosci* 32(48):17365–17372
- Pierpaoli C, Jezzard P, Basser PJ et al (1996) Diffusion tensor MR imaging of the human brain. *Radiology* 201(3):637–648
- Pugliese L, Catani M, Ameis S et al (2009) The anatomy of extended limbic pathways in Asperger syndrome: a preliminary diffusion tensor imaging tractography study. *Neuroimage* 47(2):427–434
- Qiu A, Zhong J, Graham S et al (2009) Combined analyses of thalamic volume, shape and white matter integrity in first-episode schizophrenia. *Neuroimage* 47(4):1163–1171
- Qiu A, Tuan TA, Woon PS et al (2010) Hippocampal-cortical structural connectivity disruptions in schizophrenia: an integrated perspective from hippocampal shape, cortical thickness, and integrity of white matter bundles. *Neuroimage* 52(4):1181–1189
- Rabi IIZ, Millman JR, Kusch SP (1938) A new method of measuring nuclear magnetic moment. *Phys Rev* 53(4):318
- Rathi Y, Michailovich O, Setsompop K et al (2011) Sparse multi-shell diffusion imaging. *Med Image Comput Comput Assist Interv* 14(Pt 2):58–65
- Shenton ME, Dickey CC, Frumin M et al (2001) A review of MRI findings in schizophrenia. *Schizophr Res* 49(1–2):1–52
- Smith SM, Jenkinson M, Johansen-Berg H et al (2006) Tract-based spatial statistics: voxelwise analysis of multi-subject diffusion data. *Neuroimage* 31(4):1487–1505
- Song SK, Sun SW, Ramsbottom MJ et al (2002) Demyelination revealed through MRI as increased radial (but unchanged axial) diffusion of water. *Neuroimage* 17(3):1429–1436
- Spiotta AM, Bartsch AJ, Benzel EC (2012) Heading in soccer: dangerous play? *Neurosurgery* 70(1):1–11; discussion 11
- Stejskal EO, Tanner J (1965) Spin diffusion measurements: spin echoes in the presence of time-dependent field gradient. *J Chem Phys* 42(1):288–292
- Takahashi M, Hackney DB, Zhang G et al (2002) Magnetic resonance microimaging of intraaxonal water diffusion in live excised lamprey spinal cord. *Proc Natl Acad Sci U S A* 99(25):16192–16196
- Warach S, Gaa J, Siewert B et al (1995) Acute human stroke studied by whole brain echo planar diffusion-weighted magnetic resonance imaging. *Ann Neurol* 37(2):231–241